Inorganic Chemistry

Article

pubs.acs.org/IC

Gas Sorption, Second-Order Nonlinear Optics, and Luminescence Properties of a Series of Lanthanide–Organic Frameworks Based on Nanosized Tris((4-carboxyl)phenylduryl)amine Ligand

Yan-Ping He, Yan-Xi Tan, and Jian Zhang*

State Key Laboratory of Structural Chemistry, Fujian Institute of Research on the Structure of Matter, Chinese Academy of Sciences, Fuzhou, Fujian 35002, China

Supporting Information

ABSTRACT: By controlling the pH value of the reaction system, two sets of lanthanide (Ln)–tris((4-carboxyl)-phenylduryl)amine (Ln = Ce, Pr, Nd, Sm) frameworks have been generated. Four isostructural noninterpenetrating frameworks (**FIR-8** to **FIR-11**) are constructed from rod-shaped secondary building units and four other isostructural frameworks (**FIR-12** to **FIR-15**) based on single Ln nodes are described as 8-fold interpenetrating dia-type nets. Gas sorption measurements for **FIR-8** give a Langmuir surface area of 633.8 $m^2 \cdot g^{-1}$ and a H_2 uptake of 165.2 $cm^3 \cdot g^{-1}$ at 77 K and 1 atm. However, **FIR-12** with smaller pores can hardly adsorb any N_2 and H_2. Because both **FIR-8** and **FIR-12** crystallize in acentric space group, the second-harmonic generation (SHG) measurements indicate that both of them display strong powder SHG efficiencies, which are approximately 8 and 3 times as strong as that of a potassium dihydrogen phosphate powder. In addition, the fluorescent emissions of all compounds in the solid state are also investigated in detail.

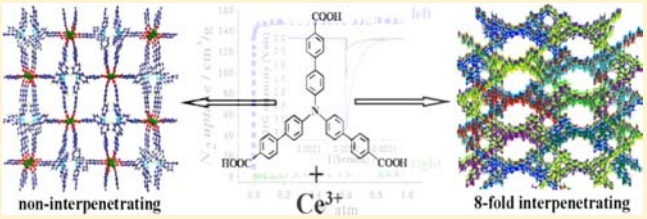

INTRODUCTION

Metal–organic frameworks (MOFs) have attracted great attention because of their aesthetic framework structures and potential applications in the fields of gas adsorption and separation,[1] nonlinear optics,[2] and photochemical areas.[3] Recently, a number of porous MOFs based on nanosized polycarboxylate ligands and metal ions have been reported,[4] but the common feature presented in these MOFs is interpenetration.[4a,e,5−7] For example, Yaghi and co-workers have reported MOF-177 built by $[Zn_4O(CO_2)_6]$ and 1,3,5-tris(4-carboxyphenyl)benzene ligand.[5] Lin et al. reported a 2-fold interpenetrating porous MOF constructed from the $[Cu_2(O_2CR)_4]$ units and methanetetra(biphenyl-*p*-carboxylic acid).[6] Interpenetration might limit the size of the pores in crystal frameworks and influence the properties, especially gas sorption. Therefore, how to avoid this interpenetrating phenomenon is challenging and significant. One effective method is to decorate the nanosized organic ligand via adding some large hindrance groups, but these hindrance groups can reduce the size of the channels. Another feasible way recently reported by Yaghi and co-workers is to use in situ generated rod-shaped metal–carboxylate secondary building units (SBUs),[8] the rigidity of the rod-shaped SBUs effectively avoids interpenetration due to the intrinsic packing arrangement of such rods in the crystal structure. As a nanosized N-centered carboxylate ligand, tris((4-carboxyl)phenylduryl)amine (H_3L) has been used to synthesize two noninterpenetrated MOFs by our group, which are also constructed by rod-shaped metal–carboxylate SBUs,[9b] but none of them were lanthanide–organic frameworks.

In this work, by employing the H_3L ligand to assemble with Ln^{3+} ions, we successfully synthesized four isostructural noninterpenetrating MOFs containing the infinite rod-shaped SBUs, namely, $[Ln(L)]\cdot 1.5H_2O\cdot 0.5EtOH\cdot DMF$ (Ln = Ce (**FIR-8**), Pr (**FIR-9**), Nd (**FIR-10**), Sm (**FIR-11**)). However, the presence of five drops of HCOOH in the reaction system gives four other isostructural 8-fold interpenetrated diamondoid MOFs built by small-sized and mononuclear SBUs, namely, $(Me_2NH_2)[Ln(HL)_2(H_2O)_2]\cdot 1.5H_2O\cdot DMF$ (Ln = Ce (**FIR-12**), Pr (**FIR-13**), Nd (**FIR-14**), Sm (**FIR-15**)). **FIR-8** shows a high permanent porosity with a Langmuir surface area of 633.8 $m^2 \cdot g^{-1}$ and a high H_2 uptake of 165.2 $cm^3 \cdot g^{-1}$ at 77 K and 1 atm. However, **FIR-12** with smaller pores can hardly adsorb N_2 and H_2. Second-harmonic generation (SHG) measurements reveal that **FIR-8** and **FIR-12** display strong powder SHG efficiencies. In addition, the fluorescent emissions of all the compounds in the solid state are also investigated.

EXPERIMENTAL SECTION

Materials and Instrumentation. All reagents were purchased commercially and used without further purification. The purity of all gases is 99.999%. All syntheses were carried out in a 20 mL vial under autogenous pressure. Diffraction data were collected by using a Bruker Smart Apex CCD diffractometer with graphite monochromated Mo Kα radiation (λ = 0.710 73 Å) at 293 K. Absorption correction was applied by using SADABS. The structure was solved by direct methods and refined by the full-matrix least-squares technique by using

Received: August 6, 2013
Published: October 24, 2013

SHELXTL.[17] All Powder X-ray diffraction (PXRD) analyses were recorded on a Rigaku Dmax2500 diffractometer with Cu Kα radiation (λ = 1.540 56 Å) with a step size of 0.05°. Thermal stability studies were carried out on a NETSCHZ STA-449C thermoanalyzer with a heating rate of 10 °C/min under a nitrogen atmosphere. Gas adsorption measurement was performed in the ASAP (Accelerated Surface Area and Porosimetry) 2020 System. Nonlinear optical (NLO) properties were measured by Kurtz–Perry powder SHG test using an Nd:YAG laser (1064 nm) with an input pulse of 350 mV. Fluorescence spectra were measured with a HORIBA Jobin-Yvon FluoroMax-4 spectrometer.

Synthesis of [Ln(L)]·1.5H_2O·0.5EtOH·DMF (Ln = Ce (FIR-8), Pr (FIR-9), Nd (FIR-10), Sm (FIR-11)). H_3L (60 mg, 0.1 mmol) and $Ln(NO_3)_3·6H_2O$ (43 mg, 0.1 mmol) were dissolved in 6 mL of DMF/EtOH/H_2O (1:1:1, v/v), and then the solution was placed in a small vial. The mixture was heated at 100 °C for 12 h and then cooled to room temperature. Yellow needlelike crystals of the product were formed and collected by filtration and then washed with DMF several times. (yield: 85% based on H_3L). The as-synthesized **FIR-8** to **FIR-11** samples are isostructural and in fine purity, as demonstrated by the similarity of their powder XRD patterns (Figure S9, Supporting Information). Elemental analysis for $C_{43}H_{37}O_9N_2Ce$ (**FIR-8**) Calcd (%): C, 59.65; H, 4.31; N, 3.24. Found: C, 59.69; H, 4.35; N, 3.25.

Synthesis of (Me_2NH_2)[Ln(HL)$_2$(H_2O)$_2$]·1.5H_2O·DMF (Ln = Ce (FIR-12), Pr (FIR-13), Nd (FIR-14), Sm (FIR-15)). H_3L (60 mg, 0.1 mmol) and $Ln(NO_3)_3·6H_2O$ (43 mg, 0.1 mmol) were dissolved in 6 mL of DMF/EtOH/H_2O (1:1:1, v/v) component solvent. Five drops of HCOOH was added to the solution to adjust the pH value (pH ≈ 4.5), and then the solution was sealed in a small vial. The mixture was heated at 100 °C for 12 h and then cooled to room temperature. Yellow sheetlike crystals of the product were formed and collected by filtration and then washed with DMF several times. (yield: 45% based on H_3L). The same powder XRD measurements were carried out to prove compounds **FIR-13**, **FIR-14**, and **FIR-15** are isostructural with **FIR-12** (Figure S10, Supporting Information). Elemental analysis for $C_{83}H_{72}N_4O_{16.5}Ce$ (**FIR-12**), Calcd (%): C, 65.17; H, 4.74; N, 3.66. Found: C, 65.21; H, 4.77; N, 3.69.

Crystal Data for FIR-8. Space group *Pnc*2, orthorhombic, a = 22.1408(6) Å, b = 24.5577(8) Å, c = 7.3445(2) Å, $\alpha = \beta = \gamma$ = 90.00°, V = 3993.4(2) Å^3, T = 293(2) K, Z = 4, 9225 reflections measured, 4564 independent reflections (R_{int} = 0.0358). The final R_1 value was 0.0663 ($I > 2\sigma(I)$). The final $wR(F^2)$ value was 0.1748 ($I > 2\sigma(I)$). The goodness of fit on F^2 was 1.108. Crystal data for **FIR-12**: space group *Aba*2, orthorhombic, a = 35.7507(7) Å, b = 16.3257(3) Å, c = 13.1559(3) Å, $\alpha = \beta = \gamma$ = 90.00°, V = 7678.5(3) Å^3, T = 293(2) K, Z = 4, 9673 reflections measured, 5397 independent reflections (R_{int} = 0.0344). The final R_1 value was 0.0577 ($I > 2\sigma(I)$). The final $wR(F^2)$ value was 0.1555 ($I > 2\sigma(I)$). The goodness of fit on F^2 was 1.044. The structures were solved by the direct method and refined by the full-matrix least-squares on F^2 using the SHELXTL-97 program.

RESULTS AND DISCUSSION

The reaction of $Ln(NO_3)_3·6H_2O$ (Ln = Ce, Pr, Nd, Sm) and H_3L ligand in a solution of DMF/EtOH/H_2O (1:1:1, v/v) at 100 °C yielded compounds **FIR-8** to **FIR-11**. Herein, only the Ce–organic framework (**FIR-8**) is described in detail. X-ray single crystal diffraction reveals that compound **FIR-8** crystallizes in the acentric *Pnc*2 space group. The asymmetric unit contains one crystallographically independent Ce^{3+} ion and one L^{3-} ligand. As shown in Figure 1a, each Ce(III) atom is nine coordinated to nine oxygen atoms from six distinct L^{3-} ligands. Each carboxyl in a L^{3-} ligand links two Ce(III) ions in a η-O,O′-μ-O,O coordination mode (Figure S2, Supporting Information). The Ce–$O_{carboxyl}$ bond lengths fall into the range of 2.435–2.595 Å, which are comparable to previously reported Ce-contained MOFs.[10] The adjacent Ce(III) ions were linked by three carboxylate groups that adopted the η-O,O′-μ-O,O coordination mode to form an infinite rod-shape

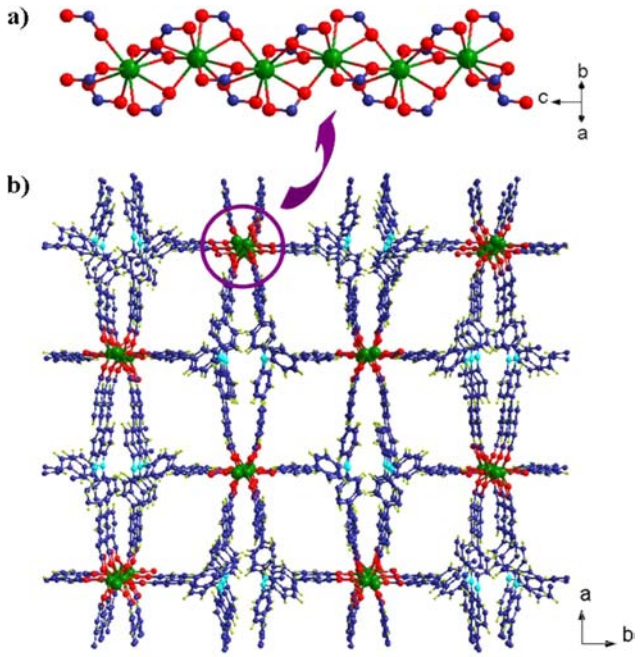

Figure 1. (a) Metal–carboxylate chain and (b) 3D framework of **FIR-8**.

$[Ce(COO)_3]_n$ chain with a Ce···Ce distance of 3.772 Å running along the c direction (Figure 1a). Each $[Ce(COO)_3]_n$ chain acts as secondary building units (SBUs) and is further connected near six chains by L ligands to form a noninterpenetrated three-dimensional (3D) architecture containing one-dimensional (1D) channels with sizes of ~7 Å viewing in the c direction (Figure 1b). Similarly to **FIR-8**, many reported MOFs constructed from rod-shaped SBUs and long multicarboxylic ligands are usually noninterpenetrated, leaving large pores or cages for gas sorption and separation.[9] The total potential void volume of open channels in **FIR-8** is about 31.8% calculated by the PLATON.

Interestingly, when five drops of HCOOH were added to the reaction system of **FIR-8** and the pH value was ~4.5, another series of Ln–tris((4-carboxyl)phenylduryl)amine frameworks (Me_2NH_2)[Ln(HL)$_2$(H_2O)$_2$]·1.5H_2O·DMF containing **FIR-12** (Ce), **FIR-13** (Pr), **FIR-14** (Nd), and **FIR-15** (Sm) were obtained. Thus, it can be seen that the pH value plays a very important role in constructing different MOFs, especially Ln MOFs. Here, the structure of **FIR-12** is selected to discuss in detail. The X-ray structure of **FIR-12** reveals an 8-fold interpenetrating dia network that is different from **FIR-8**. The crystal structure of **FIR-12** was solved in the acentric space group *Aba*2. In **FIR-12**, each Ce(III) atom is eight coordinated by six oxygen atoms from four distinct ligands and two H_2O oxygen atoms (Figure S3, Supporting Information). In fact, the incomplete deprotonated tricarboxylate ligand serves as a bent dicarboxylate linker in **FIR-12**. Thus, each HL^{2-} ligand links two Ce(III) atoms and every Ce(III) atom is connected by four HL^{2-} lignads to generate a diamond network (Figure 2a). The diamondoid cage has an edged Ce···Ce distance of 23.6 Å and a maximum Ce···Ce distance of 71.5 Å (Figure 2a). Such an unusual large cavity induces an 8-fold interpenetrating framework (Figure 2b). Up to now, a large number of interpenetrating MOFs with dia topology have been investigated and discussed,[11] but the one based on the C_3 symmetric carboxylate linker is rarely seen. The overall framework of **FIR-**

dx.doi.org/10.1021/ic4020256 | Inorg. Chem. 2013, 52, 12758–12762

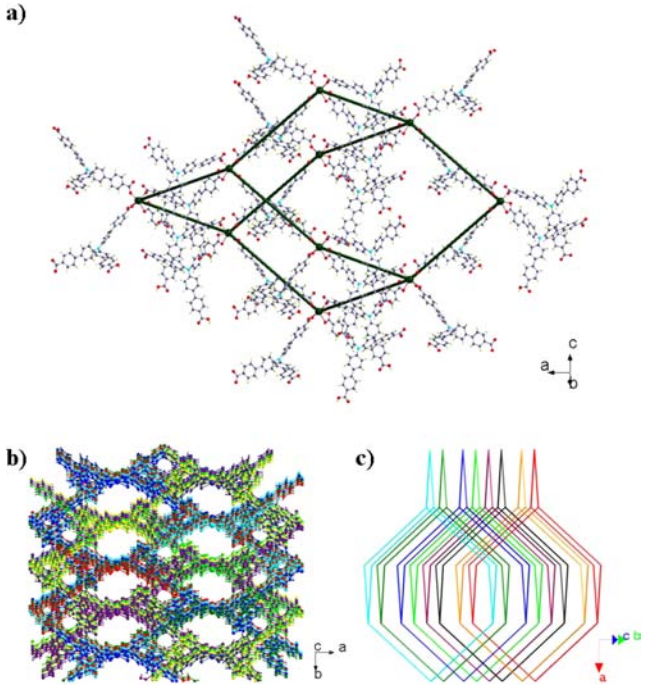

Figure 2. (a) Diamondoid cage in **FIR-12**, (b) 8-fold interpenetrating 3D architecture, and (c) view of the dia net in **FIR-12**.

12 is anionic, and each Ce^{3+} ion is corresponding to one $(Me_2NH_2)^+$ cation resolved from the decomposition of DMF solvent molecules. The solvent-accessible volume of **FIR-12** without guest and $(Me_2NH_2)^+$ cations is only 22.6% per unit cell calculated by PLATON. Apparently, small-sized, low-nuclear SBU and larger bridged ligands usually facilitate interpenetrated phenomenon, which limits the pore size and influences adsorptive properties.

The thermogravimetric analysis (TGA) curve of **FIR-8** reveals a weight loss of 14.5% in the range of 120−260 °C (Figure S5, Supporting Information), which is corresponding to one and a half H_2O, half of EtOH, and one DMF guests. The result is also determined by elemental analysis (calcd 14.21%). Only a slight weight loss is observed between 260 and 500 °C, suggesting that no chemical decomposition occurs between the desolvating and ligand-releasing temperatures. For **FIR-12**, a lower weight loss of ∼9% corresponding to the release of one and a half H_2O, one DMF, and two coordinated H_2O molecules (calcd 8.89%) can be seen (Figure S6, Supporting Information). For gas sorption studies, they were exchanged by EtOH and activated at 90 °C for 7 h under high vacuum, forming the hollow samples **FIR-8a-ht** and **FIR-12a-ht**, respectively. The PXRD patterns of two compounds before and after removing solvent confirm the keeping of porosities (Figures S7 and S8, Supporting Information).

To investigate the permanent porosity of desolvated **FIR-8a-ht** and **FIR-12a-ht**, the gas sorption experiments of N_2 and H_2 were measured at 77 K (Figure 3a). The N_2 sorption isotherm of **FIR-8a-ht** reveals a typical type-I sorption behavior and N_2 uptake of ∼149.7 $cm^3 \cdot g^{-1}$ at 1 atm, giving BET and Langmuir surface areas of 457.1 and 633.8 $m^2 \cdot g^{-1}$, respectively. However, **FIR-12a-ht** can hardly adsorb N_2 (5.4 $cm^3 \cdot g^{-1}$) and H_2 (4.7 $cm^3 \cdot g^{-1}$) because of the size-exclusion effect in the high-fold interpenetrated **FIR-12a-ht** with small pores. Compared to previous **FIR-5a-ht**,[9b] which also possesses an inorganic rod-shape chain and a Langmuir surface area of 1457 $m^2 \cdot g^{-1}$, the

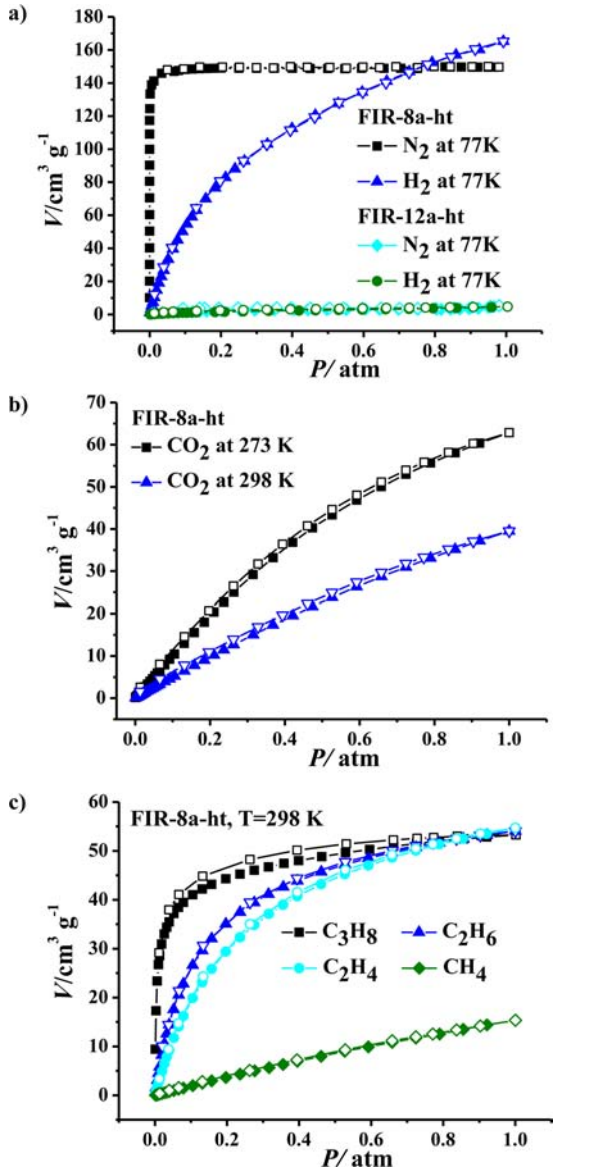

Figure 3. (a) N_2 and H_2 adsorption isotherms for **FIR-8a-ht** and **FIR-12a-ht** at 77 K, (b) CO_2 adsorption isotherms for **FIR-8a-ht** at 273 and 298 K, and (c) C_3H_8, C_2H_6, C_2H_4, and CH_4 sorption isotherms of **FIR-8a-ht** at 298 K. Solid symbols, adsorption; open symbols, desorption.

surface area of **FIR-8a-ht** is inferior. However, the H_2 uptake capacity, 165.2 $cm^3 \cdot g^{-1}$ (1.48 wt %) at 77 K and 1 atm, is higher than that for **FIR-5a-ht** (109.6 $cm^3 \cdot g^{-1}$, 0.98 wt %) and comparable to those of recently reported MOFs at the same condition.[12] In addition, the CO_2 uptakes of **FIR-8a-ht** are 63 and 39 $cm^3 \cdot g^{-1}$ at 273 and 298 K under 1 atm, respectively (Figure 3b).

We also measured the pure component sorption isotherms of various hydrocarbons for **FIR-8a-ht** at 298 K under 1 atm. As shown in Figure 3c, **FIR-8a-ht** takes up different amounts of C_3H_8 (53.3 $cm^3 \cdot g^{-1}$), C_2H_6 (54.1 $cm^3 \cdot g^{-1}$), C_2H_4 (54.7 $cm^3 \cdot g^{-1}$), and CH_4 (15.3 $cm^3 \cdot g^{-1}$) at 298 K. Although the maximum uptake of C_3H_8, C_2H_6, and C_2H_4 is significantly lower than that for MOF-74 with unsaturated metal ions under the same condition,[13] the C_2H_6 and C_2H_4 uptake capacities are better than those for UTSA-35a and UTSA-36a, as previously reported by Chen et al.[14]

dx.doi.org/10.1021/ic4020256 | Inorg. Chem. 2013, 52, 12758−12762

Because **FIR-8** and **FIR-12** crystallize in noncentrosymmetric space groups, their second-harmonic generation properties were also studied by using an Nd:YAG laser (1064 nm) (Figure 4). The second-harmonic generation (SHG) measurements were carried out on the microcrystalline samples, using 1064 nm radiation, and the results reveal that the bulk materials for **FIR-8** and **FIR-12** display strong powder SHG efficiencies, which are approximately 8 and 3 times that of a potassium dihydrogen phosphate (KDP) powder in the particle size of 125−180 μm, and further confirms their acentricity as well as evaluates their potential as second-order NLO materials. The phase matching curves are shown in Figure 4b. The SHG intensity of **FIR-8** is higher than those of $Zn(tzbc)_2$ (tzbc = 4-(1,2,4-triazol-1-yl) benzoic acid) and $(Me_2NH_2)[CdLi(odba)_2]$ (odba = 4,4′-oxidibenzoate) with 5-fold interpenetrating diamondoid networks.[15]

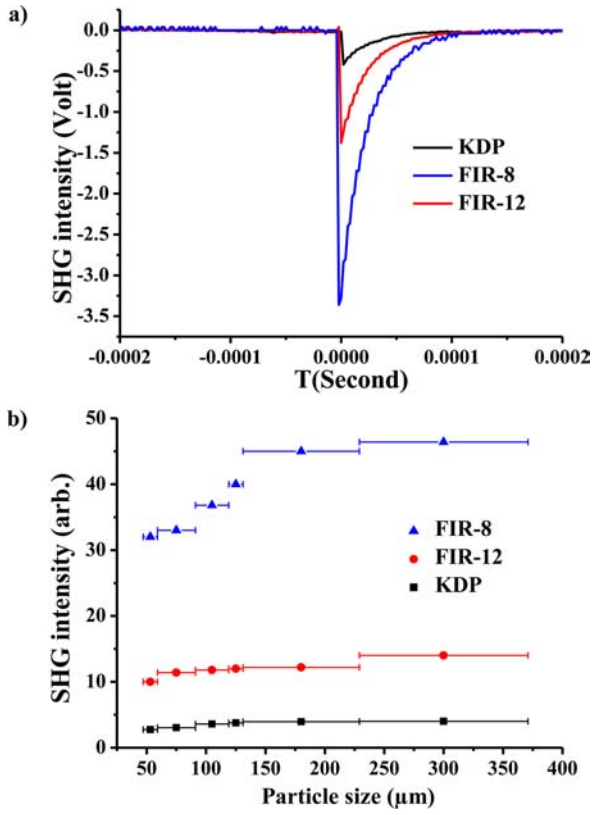

Figure 4. (a) Comparison of the measured SHG response of **FIR-8** and **FIR-12** with that of KDP at the same particle size of 125−180 μm and (b) phase-matching curves (i.e., particle size versus SHG response) for **FIR-8**, **FIR-12**, and KDP.

The solid-state emission spectra of compounds **FIR-8** to **FIR-15** together with the H_3L ligand in this work have been investigated at room temperature. It is shown that the free H_3L ligand displays the emission maxima at 494 nm, which can be assigned to the $\pi \rightarrow \pi^*$ transition (Figure 5). Apparently, all of the compounds have a peak similar to that of the ligand with a maximum absorption emission band range from 478 to 493 nm, which exhibits a slight blue-shift compared with the emission peak of the H_3L ligand. In this case, the ligand-based luminescence dominates and the blue-shifted phenomenon may possibly be attributed to the metal−ligand coordinative interactions. However, except for the ligand-based emission, compound **FIR-15** shows other four emission peaks at 558, 594, 642, and 701 nm, which are corresponding to the $^4G_{5/2} \rightarrow {}^6H_{5/2}$, $^4G_{5/2} \rightarrow {}^6H_{7/2}$, $^4G_{5/2} \rightarrow {}^6H_{9/2}$, and $^4G_{5/2} \rightarrow {}^6H_{11/2}$ characteristic transitions of the Sm^{3+} ion,[16] respectively, but these characteristic peaks are not obvious in the compound **FIR-11**. The photographs of the corresponding samples under laboratory UV light are seen in Figure S11 (Supporting Information).

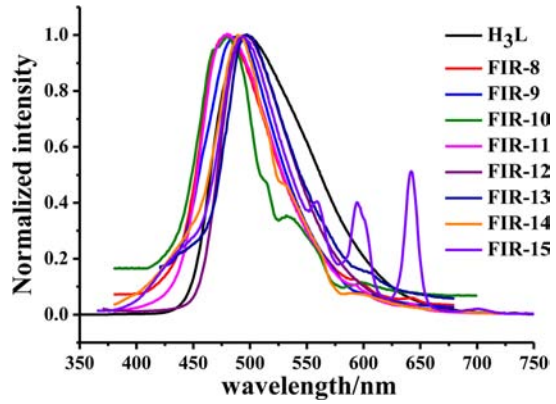

Figure 5. Solid-state emission spectra (λ_{ex} = 360 nm) measured in air at room temperature of H_3L ligand and compounds **FIR-8** to **FIR-15**.

CONCLUSION

In summary, by controlling the pH value of the reaction system, two sets of Ln−tris((4-carboxyl)phenylduryl)amine (Ln = Ce, Pr, Nd, Sm) frameworks with distinct structural features have been generated. They exhibit a noninterpenetrating rod-packing architecture (**FIR-8** to **FIR-11**) and an 8-fold interpenetrating dia-type framework (**FIR-12** to **FIR-15**), respectively. The noninterpenetrating type **FIR-8** has high surface area and high H_2 uptake capacity. However, the interpenetrating type **FIR-12** with smaller pores can hardly adsorb N_2 and H_2. Surprisingly, **FIR-8** and **FIR-12** display strong powder SHG efficiencies, which are approximately 8 and 3 times as strong as that of a KDP powder. In addition, different from other compounds, except the ligand-based emission, compound **FIR-15** also shows four characteristic emission peaks of the Sm^{3+} ion. The results reveal that these multifunctional Ln−tris((4-carboxyl)phenylduryl)amine framework materials have potential applications in gas sorption, second-order nonlinear optics and luminescence.

ASSOCIATED CONTENT

Supporting Information

Coordination environments for **FIR-8**, coordination environments and frameworks for **FIR-12**, TGA, powder X-ray diffraction patterns, luminescence photos, and CIF file. This material is available free of charge via the Internet at http://pubs.acs.org.

AUTHOR INFORMATION

Corresponding Author

*J. Zhang. E-mail: zhj@fjirsm.ac.cn. Fax: (+86)-591-83714946. Tel: (+86)-591-83715030.

Notes

The authors declare no competing financial interest.

dx.doi.org/10.1021/ic4020256 | Inorg. Chem. 2013, 52, 12758−12762

■ ACKNOWLEDGMENTS

We thank the support of this work by 973 program (2012CB821705 and 2011CB932504), NSFC (91222105, 21221001), NSF of Fujian Province (2011J06005), and CAS (XDA07070200).

■ REFERENCES

(1) (a) Liu, J.; Thallapally, P. K.; McGrail, B. P.; Brown, D. R.; Liu, J. *Chem. Soc. Rev.* **2012**, *41*, 2308−2322. (b) Suh, M. P.; Park, H. J.; Prasad, T. K.; Lim, D. W. *Chem. Rev.* **2012**, *112*, 782−835. (c) Zhang, Z. J.; Gao, W. Y.; Wojtas, L.; Ma, S. Q.; Eddaoudi, M.; Zaworotko, M. J. *Angew. Chem., Int. Ed.* **2012**, *124*, 9464−9468. (d) Jiang, H. L.; Feng, D. W.; Liu, T. F.; Li, J. R; Zhou, H. C. *J. Am. Chem. Soc.* **2012**, *134*, 14690−14693. (e) Tan, Y. X.; He, Y. P.; Zhang, J. *Chem. Commun.* **2011**, *47*, 10647−10649.

(2) (a) Yu, J. C.; Cui, Y. J.; Wu, C. D.; Yang, Y.; Wang, Z. Y.; O'Keeffe, M.; Chen, B. L.; Qian, G. D. *Angew. Chem., Int. Ed.* **2012**, *124*, 10694−10697. (b) Reinsch, H.; van der Veen, M. A.; Gil, B.; Marszalek, B.; Verbiest, T.; de Vos, D.; Stock, N. *Chem. Mater.* **2013**, *25*, 17−26. (c) Xiong, W.-W.; Athersh, E. U.; Ng, Y. T.; Ding, J.; Wu, T.; Zhang, Q. *J. Am. Chem. Soc.* **2013**, *135*, 1256−1259. (d) Chen, N.; Li, M.-X.; Yang, P.; He, X.; Shao, M.; Zhu, S.-R. *Cryst. Growth Des.* **2013**, *13*, 2650−2660. (e) Wu, L.-Z.; Cheng, L.; Shen, J.-N.; Yang, G.-Y. *CrystEngComm* **2013**, *15*, 4483−4488.

(3) (a) Cui, Y.; Yue, Y.; Qian, G.; Chen, B. *Chem. Rev.* **2012**, *112*, 1126−1162. (b) Allendorf, M. D.; Bauer, C. A.; Bhakta, R. K.; Houk, R. J. T. *Chem. Soc. Rev.* **2009**, *38*, 1330−1352. (c) Guo, Z.; Xu, H.; Su, S.; Cai, J.; Dang, S.; Xiang, S.; Qian, G.; Zhang, H.; O'Keeffe, M.; Chen, B. *Chem. Commun.* **2011**, *47*, 5551−5553. (d) Wang, Y. L.; Fu, J. H.; Wei, J. J.; Xu, X.; Li, X. F.; Liu, Q. Y. *Cryst. Growth Des.* **2012**, *12*, 4663−4668. (e) Bauer, C. A.; Timofeeva, T. V.; Settersten, T. B.; Patterson, B. D.; Liu, V. H.; Simmons, B. A.; Allendorf, M. D. *J. Am. Chem. Soc.* **2007**, *129*, 7136−7144. (f) Liu, Y.; Tan, M. J. W.; Wei, F. X.; Tian, Y. F.; Wu, T.; Kloc, C.; Huo, F. W.; Yan, Q. Y.; Hng, H. H.; Ma, J.; Zhang, Q. C. *CrystEngComm* **2012**, *14*, 75−78. (g) Liu, Y.; Boey, F.; Lao, L. L.; Zhang, H.; Liu, X. G.; Zhang, Q. C. *Chem.−Asian J.* **2011**, *6*, 1004−1006.

(4) (a) Lan, Y. Q.; Li, S. L.; Jiang, H. L.; Xu, Q. *Chem.—Eur. J.* **2012**, *18*, 8076−8083. (b) Sun, D. F.; Ke, Y. X.; Mattox, T. M.; Parkin, S.; Zhou, H. C. *Inorg. Chem.* **2006**, *45*, 7566−7568. (c) Stylianou, K. C.; Heck, R.; Chong, S. Y.; Bacsa, J.; Jones, J. T. A.; Khimyak, Y. Z.; Bradshaw, D.; Rosseinsky, M. J. *J. Am. Chem. Soc.* **2010**, *132*, 4119−4130. (d) Han, D.; Jiang, F. L.; Wu, M. Y.; Chen, L.; Chen, Q. H.; Hong, M. C. *Chem. Commun.* **2011**, *47*, 9861−9863. (e) Chen, B. L.; Eddaoudi, M.; Hyde, S. T.; O'Keeffe, M.; Yaghi, O. M. *Science* **2001**, *291*, 1021−1023. (f) Gotthardt, J. M.; White, K. F.; Abrahams, B. F.; Ritchie, C.; Boskovic, C. *Cryst. Growth Des.* **2012**, *12*, 4425−4430. (g) Gao, J. K.; He, M.; Lee, Z. Y.; Cao, W. F.; Xiong, W.-W.; Li, Y. X.; Ganguly, R.; Wu, T.; Zhang, Q. C. *Dalton Trans.* **2013**, *42*, 11367−11370.

(5) (a) Chae, H. K.; Siberio-Pérez, D. Y.; Kim, J.; Go, Y. B.; Eddaoudi, M.; Matzger, A. J.; O'Keeffe, M.; Yaghi, O. M. *Nature* **2004**, *427*, 523−527. (b) Yang, S.; Lin, X.; Blake, A. J.; Walker, G.; Hubberstey, P.; Champness, N. R.; Schröder, M. *Nat. Chem.* **2009**, *1*, 487. (c) Zheng, S.; Wu, T.; Zuo, F.; Chou, C.-T.; Feng, P.; Bu, X. *J. Am. Chem. Soc.* **2012**, *134*, 1934.

(6) Ma, L. Q.; Jin, A.; Xie, Z. G.; Lin, W. B. *Angew. Chem., Int. Ed.* **2009**, *121*, 10089−10092.

(7) (a) He, Y. P.; Tan, Y. X.; Wang, F.; Zhang, J. *Inorg. Chem.* **2012**, *51*, 1995−1997. (b) Tan, Y. X.; He, Y. P.; Zhang, J. *Cryst. Growth Des.* **2012**, *12*, 2468−2471. (c) Park, H. J.; Lim, D. W.; Yang, W. S.; Oh, T. R.; Suh, M. P. *Chem.—Eur. J.* **2011**, *17*, 7251−7260. (d) Wen, L.; Cheng, P.; Lin, W. B. *Chem. Sci.* **2012**, *3*, 2288−2292. (e) Sava, D. F.; Rohwer, L. E. S.; Rodriguez, M. A.; Nenoff, T. M. *J. Am. Chem. Soc.* **2012**, *134*, 3983−3986. (f) Men, Y. B.; Sun, J. L.; Huang, Z. T.; Zheng, Q. Y. *Chem. Commun.* **2010**, *46*, 6299−6301.

(8) Rosi, N. L.; Kim, J.; Eddaoudi, M.; Chen, B.; O'Keeffe, M.; Yaghi, O. M. *J. Am. Chem. Soc.* **2005**, *127*, 1504−1518.

(9) (a) Lin, Z. J.; Zou, R. Q.; Xia, W.; Chen, L. J.; Wang, X. D.; Liao, F. H.; Wang, Y. X.; Lin, J. H.; Burrell, A. K. *J. Mater. Chem.* **2012**, *22*, 21076−21084. (b) He, Y.-P.; Tan, Y.-X.; Zhang, J. *Cryst. Growth Des.* **2013**, *13*, 6−9. (c) Zhang, H. B.; Li, N.; Tian, C. B.; Liu, T. F.; Du, F. L.; Lin, P.; Li, Z. H.; Du, S. W. *Cryst. Growth Des.* **2012**, *12*, 670−678. (d) Li, X.-J.; Wang, X.-Y.; Gao, S.; Cao, R. *Inorg. Chem.* **2006**, *45*, 1508−1516. (e) Li, Y. W.; Zhao, J.-P.; Wang, L.-F.; Bu, X.-H. *CrystEngComm* **2011**, *13*, 6002−6006.

(10) (a) Dang, D. B.; Wu, P. Y.; He, C.; Xie, Z.; Duan, C. Y. *J. Am. Chem. Soc.* **2010**, *132*, 14321−14323. (b) Gándara, F.; de Andrés, A.; Gómez-Lor, B.; Gutiérrez-Puebla, E.; Iglesias, M.; Monge, M. A.; Proserpio, D. M.; Snejko, N. *Cryst. Growth Des.* **2008**, *8*, 378−380. (c) Han, Y. F.; Li, X. Y.; Li, L. Q.; Ma, C. L.; Shen, Z.; Song, Y.; You, X. Z. *Inorg. Chem.* **2010**, *49*, 10781−10787. (d) Sun, Y.-G.; Wu, Y.-L.; Xiong, G.; Smet, P. F.; Ding, F.; Guo, M.-Y.; Zhu, M.-C.; Gao, E.-J.; Poelman, D.; Verpoort, F. *Dalton Trans.* **2010**, *39*, 11383−11395.

(11) (a) Baburin, I. A.; Blatov, V. A.; Carlucci, L.; Ciani, G.; Proserpio, D. M. *Cryst. Growth Des.* **2008**, *8*, 519. (b) Zhang, J.; Bu, X. *Angew. Chem., Int. Ed.* **2007**, *46*, 6115. (c) He, Y.-P.; Tan, Y.-X.; Zhang, J. *CrystEngComm* **2012**, *14*, 6359−6361. (d) Men, Y.-B.; Sun, J.; Huang, Z.-T.; Zheng, Q.-Y. *CrystEngComm* **2009**, *11*, 978. (e) Hsu, Y.; Lin, C.; Chen, J.; Wang, J. *Cryst. Growth Des.* **2008**, *8*, 1094.

(12) (a) Tan, Y.-X.; He, Y.-P.; Zhang, J. *Cryst. Growth Des.* **2012**, *12*, 2468−2471. (b) Wang, Z. X.; Zheng, B. S.; Liu, H. T.; Yi, P. G.; Li, X. F.; Yu, X. Y.; Yun, R. R. *Dalton Trans.* **2013**, DOI: 10.1039/C3DT50704A. (c) Wen, L.; Cheng, P.; Lin, W. B. *Chem. Sci.* **2012**, *3*, 2288−2292.

(13) (a) Bae, Y.-S.; Lee, C. Y.; Kim, K. C.; Farha, O. K.; Nickias, P.; Hupp, J. T.; Nguyen, S. T.; Snurr, R. Q. *Angew. Chem., Int. Ed.* **2012**, *51*, 1893−1896. (b) He, Y.; Krishna, R.; Chen, B. *Energy Environ. Sci.* **2012**, *5*, 9107−9120.

(14) (a) He, Y.; Zhang, Z.; Xiang, S.; Fronczek, F. R.; Krishna, R.; Chen, B. *Chem. Commun.* **2012**, *48*, 6493−6495. (b) Das, M. C.; Xu, H.; Xiang, S.; Zhang, Z.; Arman, H. D.; Qian, G.; Chen, B. *Chem.−Eur. J.* **2011**, *17*, 7817−7822.

(15) (a) Wang, Y.-L.; Fu, J.-H.; Wei, J.-J.; Xu, X.; Li, X.-F.; Liu, Q.-Y. *Cryst. Growth Des.* **2012**, *12*, 4663−4668. (b) Lin, J.-D.; Long, X.-F.; Lin, P.; Du, S.-W. *Cryst. Growth Des.* **2010**, *10*, 146−157.

(16) Wang, P.; Fan, R.-Q.; Liu, X.-R.; Wang, L.-Y.; Yang, Y.-L.; Cao, W.-W.; Yang, B.; Hasi, W.; Su, Q.; Mu, Y. *CrystEngComm* **2013**, *15*, 1931−1949.

(17) Sheldrick, G. M. *Acta Crystallogr.* **2008**, *A64*, 112.